ORIGINAL PAPER

Well log data analysis for lithology and fluid identification in Krishna-Godavari Basin, India

Baisakhi Das[1] · Rima Chatterjee[1]

Abstract

Well log analysis provides the information on petrophysical properties of reservoir rock and its fluid content. The present study depicts interpretation of well log responses such as gamma ray, resistivity, density and neutron logs from six wells, namely W-1, W-2, W-9, W-12, W-13 and W-14 under the study area of Krishna-Godavari (K-G) basin. The logs have been used primarily for identification of lithology and hydrocarbon-bearing zones. The gamma ray log trend indicates deposition of cleaning upward sediment. Coarsening upward, clayey-silty-sandy bodies have been evidenced from the gamma ray log. Gas-bearing zones are characterised by low gamma ray, high deep resistivity and crossover between neutron and density logs. Total 14 numbers of hydrocarbon-bearing zones are identified from wells W-9, W-12, W-13 and W-14 using conventional log analysis. Crossplotting techniques are adopted for identification of lithology and fluid type using log responses. Crossplots, namely P-impedance vs. S-impedance, P-impedance vs. ratio of P-wave and S-wave velocities (Vp/Vs) and lambda-mu-rho (LMR), have been analysed to discriminate between lithology and fluid types. Vp/Vs vs. P-impedance crossplot is able to detect gas sand, brine sand and shale whereas P-impedance vs. S-impedance crossplot detects shale and sand trends only. LMR technique, i.e. $\lambda\rho$ vs. $\mu\rho$ crossplot is able to discriminate gas sand, brine sand, carbonate and shale. The LMR crossplot improves the detectability and sensitivity of fluid types and carbonate lithology over other crossplotting techniques. Petrophysical parameters like volume of shale, effective porosity and water saturation in the hydrocarbon-bearing zones in these wells range from 5 to 37%, from 11 to 36 and from 10 to 50% respectively. The estimated petrophysical parameters and lithology are validated with limited core samples and cutting samples from five wells under the study area.

Keywords Well log · Depositional environment · Crossplot technique · Petrophysical parameter · Hydrocarbon-bearing zones

Introduction

Formation evaluation is a practice of interpreting data inside a wellbore to detect and quantify hydrocarbon reserves, physical chemical properties of rock, lithology and fluid types (Hassan et al. 2013). Petrophysical study generally deals with the properties of porous media such as: porosity, permeability, water saturation, fluid identification and shaliness particularly in reservoir rock (Mukerji et al. 2001; Sarasty and Stewart 2003; Omudu et al. 2008; Inichinbia et al. 2014). Petrophysical evaluation of hydrocarbon-bearing formation generally relies on log based estimation of porosity,

permeability, mineral content and water saturation (Popielski et al. 2012). Such interpretations require calibration and validation with core data (Quirein et al. 2010). Rock physics template is another approach of identifying fluid content of reservoirs from well logs as well as seismic data (Singha and Chatterjee 2017; Datta Gupta et al. 2012). So the focus of this paper is aimed to analyse the well log responses such as gamma ray, resistivity, density, neutron, P- wave/compressional wave velocity (Vp) and S-wave/shear wave velocity (Vs) for reservoir identification and to discuss the various petrophysical parameters from six wells distributed in onshore and shallow and deep offshore parts of K-G basin. Another technique for well log analysis is crossplot technique of elastic rock properties which have been utilized to constitute better pore fill and lithology indicators. Lame's parameters (LMR: lambda—λ, mu—μ, rho—ρ) as well as P-impedance and S-impedance computed from Vp, Vs and density logs assist the identification of lithology and fluid type (Samantaray and

✉ Rima Chatterjee
   rima_c_99@yahoo.com

[1] Department of Applied Geophysics, Indian Institute of Technology (Indian School of Mines), Dhanbad, Dhanbad 826004, India

Gupta 2008; Inichinbia et al. 2014). This paper addresses on (a) identification of hydrocarbon-bearing zones from log responses, (b) computation of P-impedance, S-impedance and LMR as lithology and fluid types tools and (c) derivation of petrophysical properties mainly volume of shale, effective porosity and water saturation from available conventional log data for four wells containing few potential hydrocarbon-bearing zones ageing Early Cretaceous to Miocene.

The well-based crossplot analysis of acoustic and elastic parameters was used as a tool to establish quantitative relationship between reservoir properties and to distinguish different lithologies and fluid contents (Goodway et al. 1997, 2010). Conventional log responses such as gamma ray, resistivity, density and neutron porosity are available for five wells such as W-1, W-2, W-9, W-13 and W-14 excepting a well W-12. Resistivity logs of W-12 are not available to us. The wells namely, W-1, W-2 are located in shallow offshore, W-9, W-12are in deep offshore, W-13 is near Suryaraopeta (SUR) and Mahadevapatnam (MDH) gas fields as well as W-14is at Rangapuram (RNG) gas field under the study area (Fig. 1). These wells will be analysed in terms of petrophysical properties as mentioned above. Among six wells, Vp and Vs log data are available only for four wells: W-1, W-2, W-9 and W-12. Table 1 lists the available well log data for six wells under the study area. The lithology and fluid identification

from four wells excepting wells W-13 and W-14 are considered for P-impedance vs. Vp/Vs, P-impedance vs. S-impedance and LMR cross plotting interpretation whereas porosity crossplots are analysed for four wells.

Depositional environment from well log

The depositional environment of Early Cretaceous formation is of fluvio-deltaic setting with good sands development in channels and delta distributaries. The Late Cretaceous formations are of shallow marine setting with sand developments mostly in tidal channels, bars and sandy flats (Rao 2001; Shrivastva et al. 2008). The gamma ray and resistivity logs are called typical lithology indicative logs for siliciclastic environments (Eichkitz et al. 2009). The log shapes in gamma ray with resistivity are related to sediment character and depositional environment (Rider 2002). Shapes on the gamma ray log can be interpreted as grain size trends and by sedimentological association as cycles. Information about the sediments and sedimentary processes from the above logs may not be sufficient alone, due to some lithologies having similar natural radioactivity and electrical properties. Information from cuttings and cores is therefore often an essential component of depositional environmental analysis (Jipa 2012). A
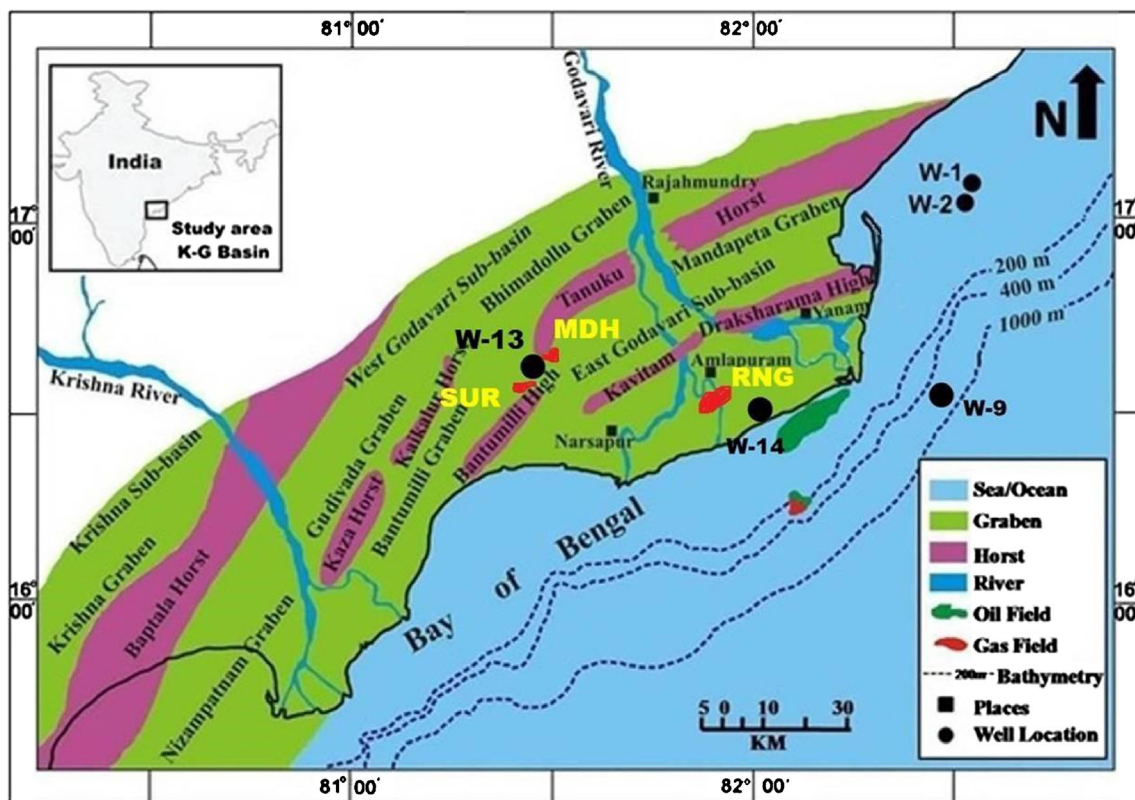

Fig. 1 The tectonic map and location of five wells distributed in the onshore and offshore of K-G basin. SUR Suryaraopeta, MDH Mahadevapatnam, RNG Rangapuram gas fields

Table 1 The available log responses of six wells distributed in K-G basin

Well	Gamma ray (API)	Resistivity (Ohm-m)		Density (gm/cm³)	Neutron porosity	Vp/Vs
		Shallow	Deep			
W-1	Y	N	Y	Y	Y	Y
W-2	Y	N	Y	Y	Y	Y
W-9	Y	Y	Y	Y	Y	Y
W-12	Y	N	N	Y	Y	Y
W-13	Y	Y	Y	Y	Y	N
W-14	Y	Y	Y	Y	Y	N

Y and N stands for availability and non-availability of data respectively

funnel shape curve indicates a coarsening upward trend. This is typical of beach sand, barrier bar sands and stream bars, which are characteristic of shore line deposits and deltaic

environment. The gamma ray log trend of W-1 (Fig. 2a) occurring between depths of 640 and 690 m is serrated and funnel-shaped with a thickness of about 50 m followed by
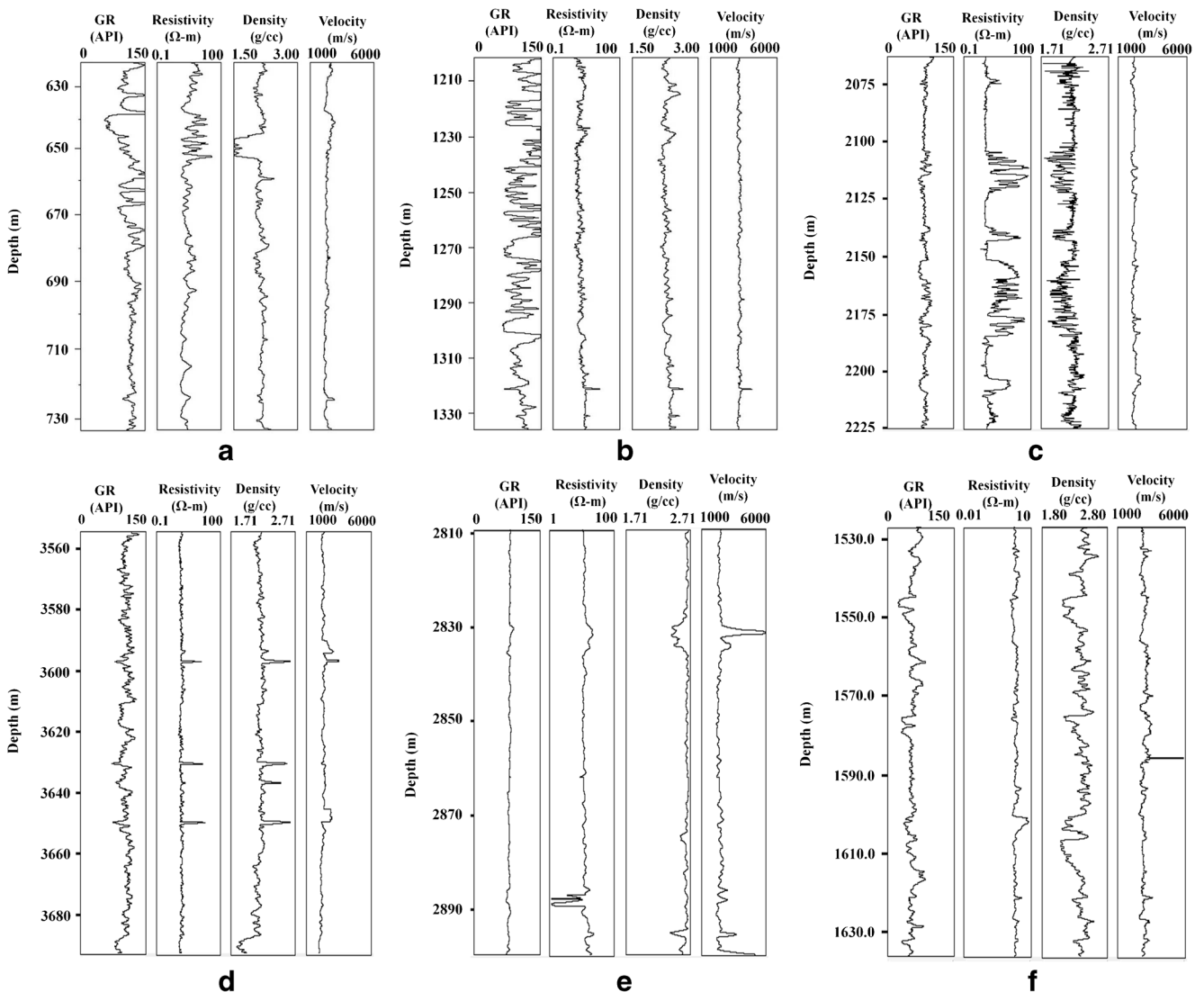

Fig. 2 Well logs. **a** W-1 well at depth intervals 620–730 m. **b** W-2 well in the depth interval of 1200–1335 m. **c** W-9 well in the depth interval of 2060–2225 m. **d** W-12 well in the depth interval of 3560–3590 m. **e** W-13

well in the depth interval of 2810–2900 m. **f** W-14 well in the depth interval of 1530–1635 m showing different depositional environments

silt/sandy silt and thick shale sequences. The depth interval of 640–642 m is characterised by resistivity of about 18 Ω-m with average porosity of 26%. The trend is usually interpreted to indicate deposition of cleaning upward sediment. According to Selley (1998), the environments of shallowing-upward and coarsening successions are divided into three categories, namely regressive barrier bars, prograding marine shelf fans and prograding delta or crevasses plays. According to Chow et al. (2005), the prograding delta is comparatively large. Funnel shaped successions in this well are showing the signature of prograding marine shelf or prograding delta (e.g. Rider 1999; Shrivastva et al. 2008; Jipa 2012). This progradation process is developed during marine transgression as reported by Rao (2001) and Bastia and Nayak (2006). Coarsening upward, clayey-silty sandy bodies, making a series of about 50 m thickness, have been evidenced from 640 to 690 m in the well log (Fig. 2a). The progradational depositional style generally contains alternating reservoir-quality sandstones interbedded with thick sealing shales as observed in northern gulf of Mexico, Niger Delta, Columbus basin, offshore Trinidad and South China sea (Leonard 1983; Ejedawe et al. 1984; Seni et al. 1994; Opara 2010; Gong et al. 2015). An extensional structural style comprising growth faults and rollover anticlines is associated with the progradational style of deposition (e.g Weber 1987; Seni et al. 1994). Figure 2b from well W-2 displays variable sandstone/silty sand body thickness patterns, including thick to thin, blocky to upward-fining log characters at greater depths (Fig. 2b). The gamma ray log shape in well W-2 displays the characteristics of singular or stacked package of sandstone/silty sand bodies of fining upward sequence (Das et al. 2017). The shallow marine environment, shallow bathymetry, very slow rate of sedimentation and the nearness to the provenance resulted in the deposition of high gamma-high resistivity shale (HG-HR) sequence (Manmohan et al. 2003). The sequence is carbonaceous, organic rich, silty and with high thorium and potassium content.

The reservoir in the interval 2212.8–2225 m in well W-9 (Fig. 2c) is an alternation of more or less shaly and silty sand which shows a megascopically coarsening up pattern up to 2222.5 m and fining up pattern above 2219 m. The next reservoir development is two coarsening up sands. These are noticed to be shaly and silty at depths of 2209.3–2211 and 2203.5–2209 m respectively. The next reservoir development is a pack of three clean sands separated by shales. The depth interval 2160.3–2175 m shows alteration of shaly sand and shale appearing as stack of coarsening up and fining up sequences with former dominating. Sand development at 2152–2160.3 m is blocky and is fining up sequence overlaying coarsening up sequence for the interval 2153–2160.3 m and blocky sand above 2153 m. The next reservoir development occurs in the interval 2137–2144 m is rapidly coarsening up sequence. The next reservoir development occurs in the interval 2104.5–2123 m; the interval is an alternation of blocky sands showing coarsening up feature dominantly. The reservoir in the interval 2072.8–2077 m is an alternation of more shaly and less shaly sands showing megascopic behaviour suggestive of coarsening up (Fig. 2c).

The gamma ray log trend of W-12 (Fig. 2d) occurring between depths of 3580–3596 and 3596–3610 m is funnel-shaped in two sequences with a thickness of about 16 and 14 m followed by silt/sandy silt and thick shale sequences. Figure 2d from well W-12 displays variable sandstone/silty sand body thickness patterns, including thick to thin, blocky to upward-fining and serrated log characters at depth intervals of 3610–3620, 3620–3640 and 3640–3680 m respectively.

The gamma ray log trend of well W-13 does not show any typical variation belonging to the depth interval 2810–2900 m (Fig. 2e).

The gamma ray log trend of W-14 (Fig. 2f) occurring between depths of 1530–1545 and 1568–1580 m is bell-shaped in two sequences with a thickness of about 15 and 12 m respectively followed by fining upward sequences. Figure 2f displays variable sandstone/silty sand body thickness patterns, including two coarsening upward and serrated log characters at depth intervals of 1545–1560, 1604–1618 and 1580–1600 m respectively.

Well log response to identify hydrocarbon reservoir

Indirect techniques for determining hydrocarbon-bearing zones are mainly based on conventional log data which are acquired by the sondes run in the exploratory well(s) (Masoudi et al. 2011). Figure 3a–f displays the typical log responses of six wells such as W-1, W-2, W-9, W-12, W-13 and W-14 respectively. The log responses of wells, namely W-9, W-12, W-13 and W-14, indicate hydrocarbon-bearing zones.

Gamma ray logs measure the radioactivity of formations in the well which connected to clay mineral, oil source rock, organic matter and shale in reservoir rock (Schlumberger 1972). Shale-free sandstones and carbonates normally have low radioactive concentrations representing relatively low gamma ray response. The gamma ray values in these hydrocarbon-bearing zones for six wells range from 43 American Petroleum Institutue (API) in W-14 well to 100API in W-9 well. Resistivity is the property of a material or substance to resist the flow of electric current (Schlumberger 1972). Three types of resistivity log are available which are flushed zone resistivity (micro spherically focussed, MSFL), shallow resistivity (laterolog shallow, LLS) and deep resistivity (laterolog deep, LLD). LLD and LLS logs show high value than MSFL logs in hydrocarbon-bearing zones. The deep resistivity log response against
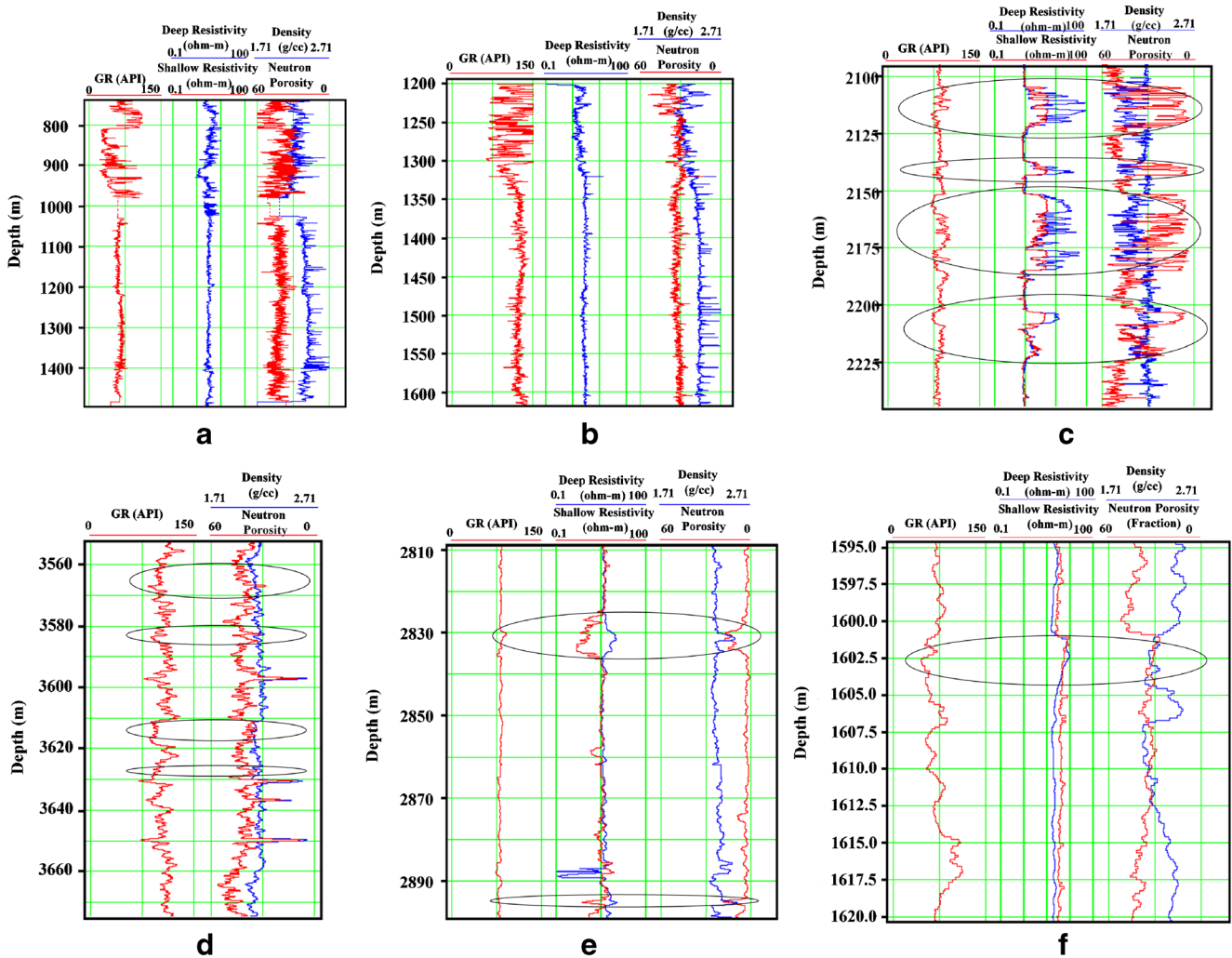
Fig. 3 Typical conventional log responses in wells. **a** W-1. **b** W-2. **c** W-9. **d** W-12. **e** W-13. **f** W-14. Hydrocarbon-bearing zones are marked by elliptical circles

hydrocarbon-bearing zones as observed from two wells out of six wells ranges from 8.0 to 36.0 Ω-m. Density log was strongly affected by the presence of gas and records the lowest density values. Neutron porosity tool accounts the amount of hydrogen present in the formation. In clean, shale-free formations, where the porosity is filled with water or oil, the neutron log measures liquid filled porosity. Neutron log response becomes high in shale because of presence of capillary and clay bound water, whereas it shows very low value in gas saturated sand.

Gas-bearing zone is indicated when the neutron porosity is less than the density porosity in a porous and permeable zone. This separation between neutron and density termed as crossover is an identification for gas-bearing zones in clean sand (Bateman 1985). The crossover becomes close to each other indicating signature of oil saturated sand and when they are overlaid with each other representing water saturated sand (Fig. 3). The log signatures in wells W-9, W-12, W-13 and W-14 (Fig. 3c–f) indicate hydrocarbon-bearing zones

in shaly sand in Raghavapuram Shale and clean sand Vadaparru Shale formation respectively. Hydrocarbon-bearing zone characterises with deep resistivity ranging 5.0 to 8.0 Ω-m, and neutron-density crossovers are observed in W-9, W-12, W-13 and W-14 respectively. Gas-bearing zones characterising average deep resistivity ranging from 20 to 173 Ω-m with good crossover between neutron and density logs are observed in wells W-9, W-13 and W-14. Gas-bearing zones are observed in Raghavapuram Shale for well W-9 and W-13, and oil-bearing zone is observed in Vadaparru Shale for well W-14. The thick layer of clean gas sands in wells W-9 and W-13 are characterised by low gamma ray (GR), higher resistivity (LLD) and good neutron-density crossover (Fig. 3c, e).

Therefore, hydrocarbon-bearing zones from four wells are identified from analysis of conventional logs. The selected depth intervals containing hydrocarbon-bearing zones are analysed with different crossplotting techniques for further discrimination of lithology and fluid types.

Lithology and fluid identification from crossplot technique

Sensitivity of reservoir rocks with respect to pore fluid is a function of porosity, fluid type and rock composition such as shale volume in sandstone (Goodway et al. 1997), and it is determined by the variation of basic rock properties: velocities and density. Other rock properties such as impedances and LMR ($\lambda\mu\rho$) are derived from these basic rock properties. Individual rock property responds differently or has different sensitivity to a given lithology or fluid contrast. Basic rock physics relations such as velocity, porosity, impedances, Lame's parameters and Vp/Vs among others are generally defined for the lithofacies (Inichinbia et al. 2014). Crossplots are visual representations of the relationship between two or more variables, and they are used to visually detect anomalies which could be interpreted as the presence of fluid types and lithologies.

As an example, log responses of six wells (W-1, W-2, W-9, W-12, W-13 and W-14) have been shown here (Fig. 3). The crossplots between elastic parameters such as P-impedance vs. S-impedance, Vp/Vs vs. P-impedance and lambda-rho ($\lambda\rho$) vs. mu-rho ($\mu\rho$) have been generated for four wells, namely W-1, W-2, W-9 and W-12 to separate the fluid types and lithology. The values of Vp/Vs are available only for the depth intervals 800 to 1400 m, 1200 to 1700 m, 1660 to 2400 m and 3443 to 4043 m from wells W-1, W-2, W-9 and W-12 respectively for crossplotting study.

Crossplot: P-impedance vs. S-impedance

P-impedance or acoustic impedance (AI) is the product of P-wave velocity and density and traditionally is a popular technique for lithology and pore fluid prediction (Pendrel and Riel 2000). S-impedance or shear impedance is the product of S-wave velocity and density. The interpretation of P-impedance vs. S-impedance crossplot is a key to understand the lithology and behaviour of sands with different fluids. The presence of gas causes decrease in P-wave velocity and density. As a consequence, there is a reduction in AI in gas saturated sand compared to the surrounding non-reservoir area (shale and shaly sand). Figure 4 displays the crossplot between P-impedance and S-impedance with gamma ray colour coding. The trendline for shale is clearly observed in all four wells W-1, W-2, W-9 and W-12.There is a clear separation between the sand and shale trend in wells W-9 and W-12 as displayed in Fig. 4c, d. Brine sands show much higher P-impedances than that of the gas sands in wells W-9 and W-12 as shown in Fig. 4c, d.

Crossplot: Vp/Vs and P-impedance

The ratio between P wave and S wave velocity (Vp/Vs) is key issue for determination of lithology from seismic or log data

and for direct seismic identification of pore fluid as well as estimation of rock mechanical properties (Avseth et al. 2005; Das and Chatterjee 2017). The P-wave velocity is more sensitive to fluid changes than the S-wave velocity. Compressional velocities travel through both rock and fluid and are slower in gas, as compared to water. In contrast, S-wave velocity is mostly insensitive to fluids and only moves through the rock. This means that the differences in the Vp/Vs ratio inside reservoir would indicate different fluid saturation (Mukerji et al. 2001). Here a significant drop in the Vp/Vs ratio shows the presence of hydrocarbon (gas sand reservoir). For instance, it is observed from several studies that the value of Vp/Vs in the gas saturated reservoir is approximately 1.62 while brine saturated sand has a Vp/Vs ratio value about 1.83 (e.g. Inichinbia et al. 2014). The relation between Vp/Vs and P-impedance separates not only the sand/shale lithology but also fluid types and hence improves discrimination between pore fluids in the sandstone reservoirs. The gas sand, brine sand and shale are distinguished in these crossplot for well W-9 and W-12 as shown in Fig. 5c, d. Gas sands observed in the wells W-9 and W-12 belong to Narasapur Claystone of Miocene age. These crossplots are better than the previous cross plotting techniques to identify lithology and fluid types.

Crossplot: lambda-rho vs. mu-rho

Goodway et al. (1997) proposed a method to extract rock properties using of relationship between Lame's parameters λ (incompressibility), μ (rigidity) and ρ (density). λ and μ are obtained from Eqs. (1) and (2). Hence, LMR (lambda-mu-rho) approach can be used to separate lithologies and to identify gas sands. Rigidity is defined as the resistance to strain resulting in shape change with no volume change. Quartz is the dominant mineral in the sand matrix; therefore, sandstone is usually associated with high rigidity than shale and coal (Goodway et al. 1997). The most interesting result from this principle is that sand matrix has higher value of mu-rho ($\mu\rho$) than the overlying shale. Incompressibility is a very useful parameter to distinguish fluid content which is subjected to pore fluid (Samantaray and Gupta 2008).Several studies have been indicated that sandstone containing hydrocarbon is less dense than sandstone containing water and also are more compressible than wet sandstone. As a result, in gas sand reservoir, the lambda-rho ($\lambda\rho$) log shows low incompressibility values. Regarding the rigidity and incompressibility, gas sand reservoir should correspond to the low λ incompressibility (< 20 GPa) combined with high rigidity μ (>15 GPa) of sand grain. The following equations are useful to calculate $\lambda\rho$ and $\mu\rho$.

$$Z_S^2 = (\rho V_S)^2 = \mu\rho \tag{1}$$

$$Z_P^2 = (\rho V_P)^2 = (\lambda + 2\mu)\rho \Longrightarrow \lambda\rho = Z_P^2 - 2Z_S^2 \tag{2}$$
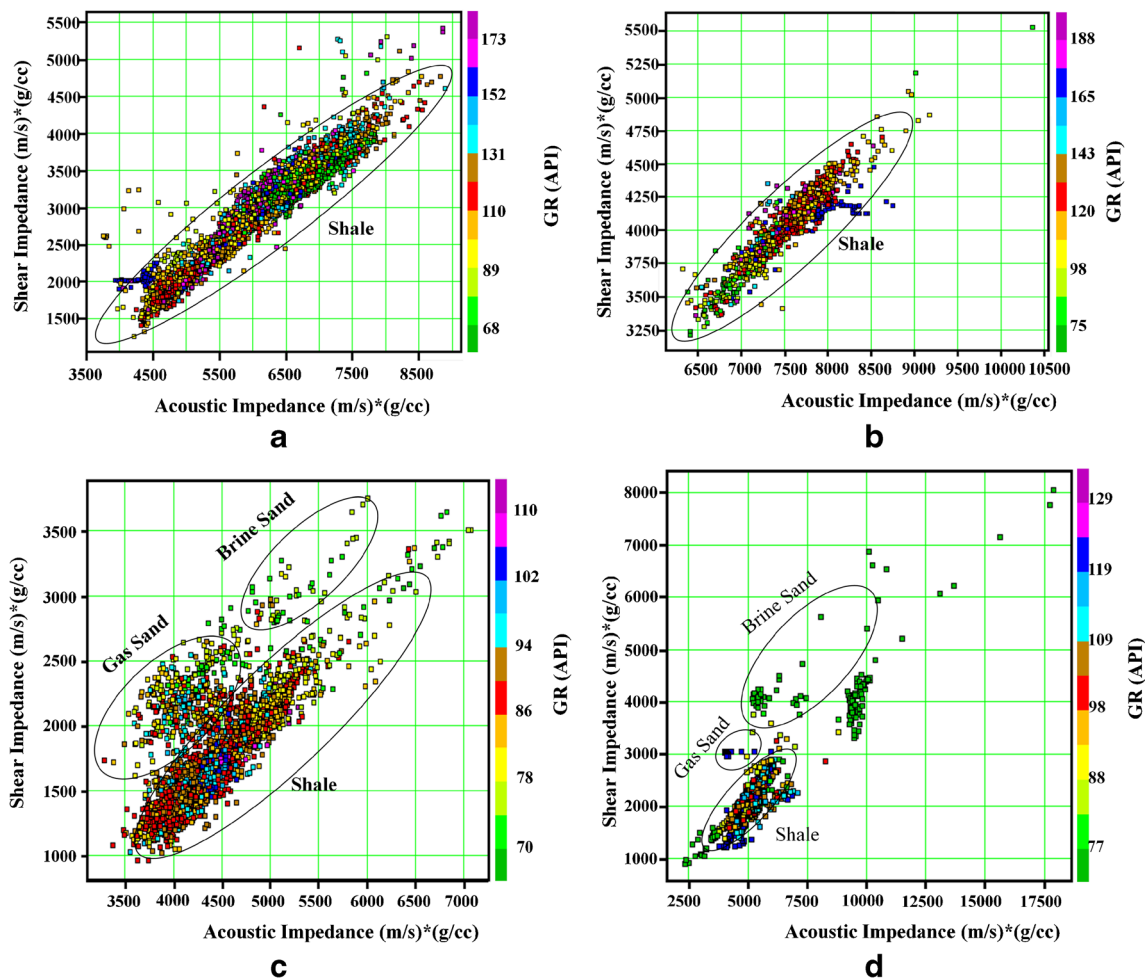
Fig. 4 Crossplot between P-impedance and S-impedance for wells. **a** W-1 for depth interval 800 to 1400 m. **b** W-2 for depth interval 1200 to 1700 m. **c** W-9 for depth interval 1660 to 2400 m. **d** W-12 for depth interval 3443 to 4043 m

where Z_P and Z_S are the P-impedance and S-impedance respectively.

Crossplotting between $\lambda\rho$ vs. $\mu\rho$ is generally believed to be better hydrocarbon indicators than the crossplot using P-impedance and S-impedances. Therefore, good discrimination of sandstone and shales is possible on the basis of rigidity where high rigidity discriminates sandstones from shales.

Different lithology and fluid types are clearly noticeable and identifiable for the well W-1, W-2, W-9 and W-12 (Fig. 6a–d). Carbonates are separated from shale in well W-12 (Fig. 6d). The carbonate lithology is found to be with greater value of $\lambda\rho$ (> 100 GPa) with varying $\mu\rho$ of 50 to 70 GPa. Shale sand and carbonate lithologies are separated in the crossplot for well W-12 (Fig. 6d). Previous crossplots are not able to detect carbonate in well W-12. Hence, this crossplot improves the detectibility and sensitivity of fluid types and carbonate lithology over other crossplotting techniques discussed above.

Determination of petrophysical parameters

Shale volume

Shale is usually more radioactive than sand or carbonate. Volume of shale can be calculated from the different log such as gamma ray, neutron and density log and can indicate the presence or absence of clay. The volume of shale (V_{sh}) is expressed as a fraction or percentage. In general, the V_{sh} log shows very low value in clean facies like sand while high V_{sh} value is interpreted as clay rich facies such as shale.

Several relationships exist for V_{sh} calculation from gamma ray log as a linear response (Fertl and Frost 1980).

$$V_{sh} = \frac{(GR - GR_{min})}{(GR_{max} - GR_{min})} \quad (3)$$

where GR = gamma ray log reading at any depth, GR_{min} = minimum gamma ray reading and GR_{max} = maximum gamma
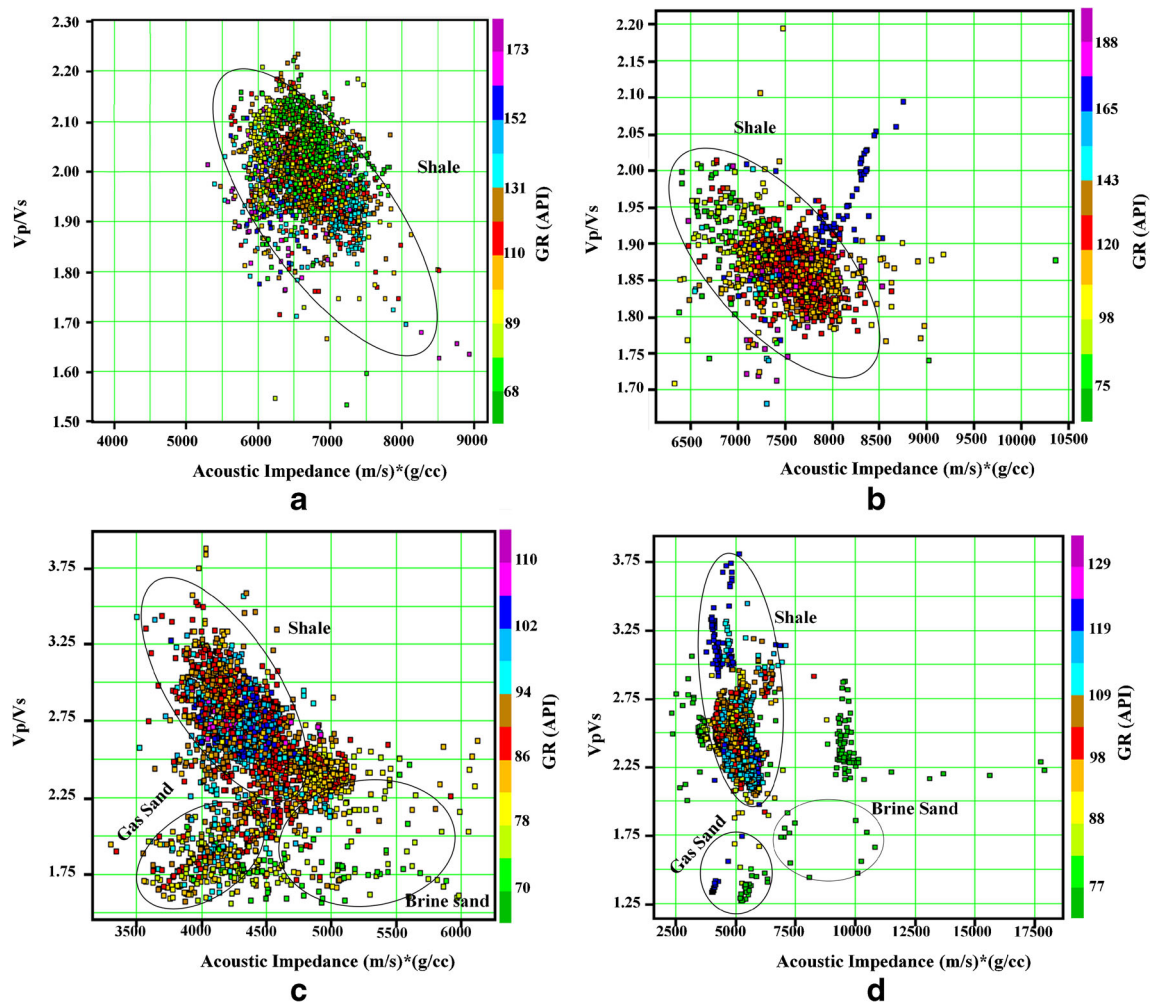
Fig. 5 Crossplot between Vp/Vs and P-impedance. **a** W-1 for depth interval 800 to 1400 m. **b** W-2 for depth interval 1200 to 1700 m. **c** W-9 for depth interval 1660 to 2400 m. **d** W-12 for depth interval 3443 to 4043 m

ray reading. GR_{min} varies from 17 to 26 API and GR_{max} from 142 to 182 API in four wells.

The value of V_{sh} listed in Table 1 ranges from 12 to 37 in shaly sand reservoirs. The value of V_{sh} below 10% represents clean sand reservoir. Gas-bearing clean sandstone reservoir occurring at depth interval 2151–2185 m thickening 34 m is identified from well W-9.

Effective porosity

Porosity is the fraction of the total volume of a rock that is free from the solid constituents. There are several types of porosity that are available such as total porosity, secondary porosity and effective porosity. Total porosity consists of the entire void spaces, i.e. pores, channels, fissures and vugs in the rock. It sums of two components: primary porosity, which is intergranular or intercrystalline. It depends on the shape, size and arrangement of the solids. And the secondary porosity was made up of vugs caused by dissolution of the matrix and fissures or

cracks caused by mechanical forces. Previously, authors are mapped total porosity of Raghavapuram shale in seismic section where it ranges from 13 to 25% (Kumar et al. 2016). Effective porosity is mainly used in log analysis for computation of water saturation. It is the porosity that is accessible to free fluids, and this porosity is internally connected to all the pore space in the rock to flow the fluid like gas, oil and water. Neutron and density log are the main logs to be used to calculate porosity. Neutron log gives the direct total porosity of the rock and whereas the density log provides porosity value by using following formula (Asquith and Gibson 1983)

$$\text{Density porosity } (\varphi d) = \frac{\left(\rho_{ma} - \rho_{log}\right)}{\left(\rho_{ma} - \rho_{fluid}\right)} \quad (4)$$

ρ_{ma} = matrix density = 2.71 g/cm^3, ρ_{fluid} = density of fluid = 1 g/cm^3 and ρ_{log} = bulk density read from density log in grams per cubic metre.
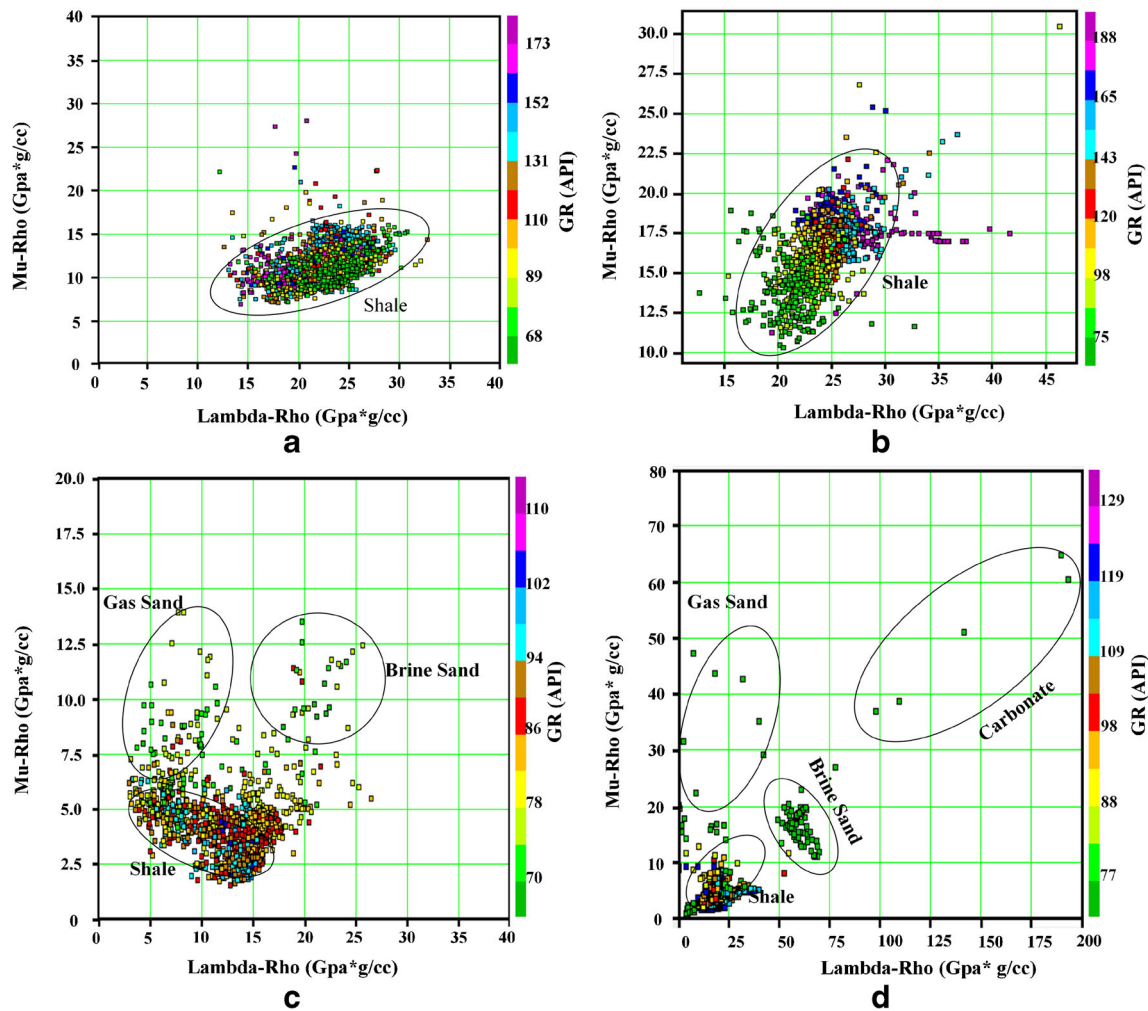
Fig. 6 Crossplot between lambda-rho ($\lambda\rho$) and mu-rho ($\mu\rho$). **a** W-1 for depth interval 800 to 1400 m. **b** W-2 for depth interval 1200 to 1700 m. **c** W-9 for depth interval 1660 to 2400 m. **d** W-12 for depth interval 3443 to 4043 m

Combining neutron and density porosity, total porosity could be obtained. So, the total porosity equation in the absence or presence of gas in the rock is as follows (Schlumberger 1972; Bateman 1985)

$$\varnothing_T = \frac{\varnothing_N + \varnothing_D}{2} \qquad (5)$$

without gas-bearing zones

$$\varnothing_T = \sqrt{\frac{\varnothing_N^2 + \varnothing_D^2}{2}} \qquad (6)$$

for gas-bearing zones.

So, effective porosity is given by using Eqs. (5) and (6)

$$\varnothing_e = \varnothing_T \times (1 - V_{sh}) \qquad (7)$$

The effective porosity (φ_e) values range from 11% in well W-13 to 28% in well W-9 as listed in Table 1. It is noted that high porosity is observed at shallow depth in wells W-9, whereas the less porosity is observed at deeper depth in well W-13.

Water saturation

The fraction of water in pore space corresponding to the effective porosity is called as water saturation (S_w). It is the most crucial petrophysical parameter for quantifying the presence of hydrocarbon in the reservoir. A number of independent approaches can be applied to estimate the S_w. Archie's equation (Archie 1942) is generally used for clean sand in which clay mineral content is low (below 10% of V_{sh}). But due to increases of shaliness in sand or clay rich sand, this model overestimates value of S_w. In case of shaly sand interpretation Poupon and Leveaux (1971) have empirically modelled field log data d to

estimate water saturation. Water saturation using this model can be written as follows:

$$S_{\mathrm{w}} = \left\{ \left[\left(\frac{V_{\mathrm{sh}}^{2-V_{\mathrm{sh}}}}{R_{\mathrm{sh}}} \right)^{1/2} + \left(\frac{\varnothing_{\mathrm{e}}^{\mathrm{m}}}{R_{\mathrm{w}}} \right)^{1/2} \right]^2 R_{\mathrm{t}} \right\}^{-1/n} \tag{8}$$

where $\varnothing_e$ = effective porosity; V_{sh} = shale volume; R_{w} = water resistivity computed from spontaneous potential (SP) log, varying from 0.02 to 0.03 Ω-m; R_{t} = deep resistivity value noted from LLD or induction log deep (ILD) whichever is available; m = cementation factor of the rock equal to 2; and n = saturation exponent assumed as 2.

The water saturation has been estimated in the identified hydrocarbon-bearing zones from four wells using Eq. (8) as shown in Table 1. The minimum value of S_{w} is found to be 10% for depth interval 2136–2145 m in W-9 well, and maximum value of S_{w} is observed as 45% for depth interval 2213–2225 m in W-9 well.

Results and discussion

The effective porosity and water saturation as listed in Table 2 indicate the indentified hydrocarbon potential zones with respective geologic age. The crossplot analysis is indeed a sophisticated interpretational tool for analysing and understanding how elastic rock properties are related and their sensitivity to various lithologies and fluid effects. LMR technique is a very important crossplot technique where the data are clustered in such way that the gas sand, brine sand, shale and carbonates are discriminated very easily but oil sand is not detected. Reservoir sands are classified on basis of fluid content from Vp/Vs vs. P-impedance and $\lambda\rho$ vs. $\mu\rho$ crossplots. The petrophysical parameters such as volume of shale, effective porosity and water saturation have been estimated using the empirical relation to evaluate and characterise the reservoir. The hydrocarbon-bearing zones are identified in onshore wells W-13 near SUR and MDH fields, W-14 at RNG field, as well as gas-bearing offshore wells W-9 and W-12.

The estimated petrophysical parameters such as porosity, water saturations and lithology are validated with very limited core samples from wells W-9 and W-14 (Source: Unpublished Reports). Cutting samples are available for wells W-1, W-2 and W-13 (Source: Unpublished Reports). No core samples/cutting samples are available for well W-12.

W-1 The dominant lithology obtained from the cutting samples from depth interval 1027–1400 m is claystone along with shale, sandstone and siltstone. Water saturation is more than 90%.

Table 2 Hydrocarbon-bearing zones identified from conventional log analysis with petrophysical parameters from nine wells of K-G basin

Wells	Depth interval (m)	Thickness (m)	Petrophysical parameters			Fluid type	Fields	Formation	Geological age
			V_{sh} (%)	Effective porosity (%)	Water saturation (%)				
W-9	2072.0–2078.0	6	36	22	35–50	Gas	Deepwater	Narasapur claystone	Miocene
	2109.0–2124.0	15	20	5–28	18				
	2136.0–2145.0	9	30	9–26	10–22				
	2151.0–2185.0	34	5–20	6–28	10–45				
	2203.5–2209	5.5	10	20	22–35				
	2213.0–2225.0	12	20–32	15–25	27–45				
W-12[a]	3560.0–3572.0	12	31–37	24	–	Gas	Deepwater	Narasapur claystone	Early Miocene
	3582.0–3586.0	4	32	20	–				
	3612.0–3618.0	6	30	22	–				
	3626.0–3630.0	4	28	22	–				
	3854.0–3856	2	12	36	–				
W-13	2829–2832	3	27	11	24	Gas	Between SUR and MDH	Raghavapuram shale	Early Cretaceous
	2894–2897	3	32	12	30				
W-14	1601–1603	2	20	22	25	Oil	Near RNG	Vadaparru shale	Early Cretaceous

[a] Water saturation of formation is not calculated due to unavailability of true resistivity log for well W-12

W-2 The dominant lithology from cutting sample from depth interval 1205–1600 m is characterised by the occurrence of thick beds of claystone with thin intercalations of siltstone, sandstone and shale with water saturation more than 90%.

W-9 The cutting samples from 2152.0 to 2175.0 m show alteration of clear and more clayey sand lithology. The porosity obtained from a core sample from 2152.0 to 2175.0 m is 30% and water saturation 18%. Hydrocarbon fluorescence test shows the presence of gas in this depth interval.

W-12 Conventional coring was not done, and cutting samples were not collected for this well.

W-13 Cutting samples were collected during drilling from surface to target depth at 3044 m. No conventional core was cut in this well, and side wall cores were not taken. The Raghavapuram shale unit encountered in this well mainly composes of claystone and splintery shale with few sandstones. Previously, Kumar et al. (2016) has mapped total porosity ranging 13–25% in post-stack seismic section from a shallow offshore well in this K-G basin.

W-14 Two core samples were collected from Vadaparru Shale for depth intervals 1481–1485 and 1503–1511 m respectively. Lithology is argillaceous sandstone or claystone. The sandstone core gives the information of porosity in the range of 25–30%, and water saturation is within 30–60%.

The porosity and water saturation values interpreted from well log analysis for wells W-9 and W-14 match well with the core test data of selected hydrocarbon-bearing zones. The effective porosity interpreted from logs of well W-13 is varying 11–12%, less than the total porosity of Raghavapuram shale mapped previously in seismic section. The lithology identified using the crossplotting technique is in close agreement with the cutting samples analysis for above-mentioned wells.

Conclusions

The crossplots like P-impedance vs. S-impedance is able to detect sand and shale trend, P-impedance vs. Vp/Vs detects brine sand, gas sands and shale. The crossplot $\lambda\rho$ vs. $\mu\rho$ is more effective for discriminating lithologies such as brine sand, gas sand, shale and carbonates with fluid content. The petrophysical parameters such as volume of shale, effective porosity and water saturation have been estimated in the hydrocarbon-bearing zones thickening 2–34 m for four wells. The volume of shale, effective porosity and water saturation in the hydrocarbon-bearing zones in these wells range from 5 to 37%, from 11 to 36% and from 10 to 50% respectively. The estimated petrophysical parameters and lithology are validated with limited core samples and cutting samples from five wells under the study area. The core samples or cutting samples support interpreted results obtained from well log data.

References

Archie GE (1942) The electrical resistivity log as an aid in determining some reservoir characteristics. Trans AIME 146(1):54–62

Asquith, G. and Gibson, C., 1983, Basic well log analysis for geologists. AAPG methods in exploration series, Tulsa, pp.216

Avseth P, Mukerji T, Mavko G (2005) Quantitative seismic interpretation: applying rock physics to reduce interpretation risk. Cambridge University Press, Cambridge, U.K.

Bastia R, Nayak P (2006) Tectonostratigraphy and depositional patterns in Krishna offshore basin, Bay of Bengal. Lead Edge 25:839–845

Bateman RM (1985) Openhole log analysis and formation evaluation. Prentice Hall PTR, New Jersey, p 647

Chow JJ, Li M-C, Fuh S (2005) Geophysical well log study on the paleo environment of the hydrocarbon producing zones in the Erchungchi Formation, Hsinyin, SW Taiwan. TAO 16:531–543

Das B, Chatterjee R (2017) Wellbore stability analysis and prediction of minimum mudweight for few wells in Krishna-Godavari Basin, India. Int J Rock Mech Min Sci 93:30–37

Das B, Chatterjee R, Singha DK, Kumar R (2017) Post-stack seismic inversion and attribute analysis in shallow offshore of Krishna-Godavari basin, India. J Geol Soc India 90:32–40

Datta Gupta S, Chatterjee R, Farooqui MY (2012) Rock physics template (RPT) analysis of well logs and seismic data for lithology and fluid classification in Cambay basin. Int J Earth Sci 101(5):1407–1426

Eichkitz CG, Schreilechner MG, Amtmann J, Schmid C (2009) Shallow seismic reflection study of the Gschliefgraben landslide deposition area—interpretation and three dimensional modeling. Aust J Earth Sci 102:52–60

Ejedawe JE, Coker SJL, Lambert-Aikhionbare DO, Alofe KB, Adoh FO (1984) Evolution of oil-generative window and oil and gas occurrence in Tertiary Niger Delta Basin. AAPG Bull 68:1744–1751

Fertl, W. and Frost, E., 1980, Evaluation of shaly clastic reservoir rocks. Journal of Petroleum Technology, September, pp. 1641-1645

Gong C, Wang Y, Steel RJ, Olariu C, Xu Q, Liu X, Zhao Q (2015) Growth styles of shelf-margin clinoforms: prediction of sand- and sediment-budget partitioning into and across the shelf. J Sediment Res 85:209–229

Goodway, B., Chen T. and Downtown, J 1997, Improved AVO fluid detection and lithology discrimination using Lame petrophysical parameters, 67th Annual international Meeting, SEG, Expanded Abstracts, 183–186

Goodway B, Perez M, Varsek J, Abaco C (2010) Seismic Petrophysics and isotropic-anisotropic AVO methods for unconventional gas exploration. Lead Edge 29:1500–1508

Hasan MM, Akter F, Deb PK (2013) Formation characterization and identification of potential hydrocarbon zone for titas gas field, Bangladesh using wireline log data. Int J Sci Eng Res 4(5): 1512–1518

Inichinbia S, Sule PO, Ahmed AL, Hamaza H, Lawal KM (2014) Petro physical analysis of among hydrocarbon field fluid and lithofacies using well log data. J Appl Geol Geophysics 2:86–96

Jipa CD (2012) Coarsening upward sedimentation in the Middle Pontian Dacian Basin, prograding shoreline or delta front? Geo-Eco-Marina 18:45–64

Kumar R, Das B, Chatterjee R, Sain K (2016) A methodology of porosity estimation from inversion of post-stack seismic data. Jf Nat Sci Eng 28:356–364

Leonard R (1983) Geology and hydrocarbon accumulations, Columbus Basin, offshore Trinidad. AAPG Bull 67:1081–1093

Manmohan M, Rao MRR, Kamraju AVVS, Yalamarty Y (2003) Origin and occurrence of Lower Cretaceous high gamma-high resistivity (Raghavapuram) shale—a key stratigraphic sequence for hydrocarbon exploration in Krishna-Godavari Basin, A.P. J Geol Soc India 62:271–289

Masoudi P, Tokhmechi B, Zahedi A, Jafari MA (2011) Developing a method for identification of net zones using log data and diffusivity equation. J Mining Environ 2(1):53–60

Mukerji T, Avseth P, Mavko G, Takahashi I, González EF (2001) Statistical rock physics: combining rock physics, information theory, and geostatistics to reduce uncertainty in seismic reservoir characterization. Lead Edge 20(3):313–319

Omudu, LM., Ebeniro, JO., Xynogalas, M., Osayande, N. and Olotu, S., 2008, Fluid discrimination and reservoir characterization from onshore Niger Delta, Society of Exploration Geophysicists, Annual General Meeting, Las Vegas, 2001–2005

Opara AI (2010) Prospectivity evaluation of ussol field, onshore Niger Delta Basin, using 3-D seismic and well log data. Pet Coal 52:307–315

Pendrel, J. and Riel, P V., 2000, Estimation and interpretation of P and S impedance volumes from simultaneous inversion of P-wave offset seismic data, Society of Exploration Geophysicists, Expanded Abstracts, 1–4

Popielski, A C., Heidari, Z., Verdin, C T., 2012, Rock classification from conventional well logs in hydrocarbon-bearing shale, SPE 159255, October, San Antonio

Poupon, A. and Leveaux, J., 1971, Evaluation of water saturation in shaly formations, Trans. SPWLA 12th Annual Logging Symposium, pp.1–2

Quirein, J., Witkowsky, J., Truax, J. A., Galford, J. E., Spain, D. S. and Odumosu, T., 2010, Integrating core data and wireline geochemical data for formation evaluation and characterization of shale-gas reservoirs, SPE annual technical conference and exhibition, Paper id SPE-134559

Rao GN (2001) Sedimentation, stratigraphy, and petroleum potential of Krishna-Godavari basin, East Coast of India. AAPG Bull 85: 1623–1643

Rider, M H., 1999, Geologic interpretation of well logs. Whittles Publishing Services

Rider, M H., 2002, The geological interpretation of well logs, 2nd edition. Rider-French Consulting Ltd, pp.280

Samantaray, S. and Gupta, P., 2008, An interpretative approach for gas zone identification and lithology discrimination using derivatives of $\lambda * \rho$ and $\mu * \rho$ attributes, 7th Biennial International Conference and Exposition on Petroleum Geophysics, Society of Petroleum Geophysicists, Hyderabad, 386–341

Sarasty, J J. and Stewart, R R., 2003, Analysis of well-log data from the white rose oilfield, offshore Newfoundland, CREWES Research Report, 15

Schlumberger, 1972, The essentials of log interpretation practice, Services Techniques Schlumberger, pp. 58

Selley, R C., 1998, Elements of petroleum geology. Department of Geology, Imperial College, London, 37-145

Seni SJ, Desselle BA, Standen A (1994) Scope and construction of a gas and oil atlas series of the Gulf of Mexico: examples from Texas offshore lower Miocene plays. Gulf Coast Assoc Geol Soci Trans 44:681–690

Shrivastava, C., Ganguly, S. and Khan, Z., 2008, Reconstructing sedimentary depositional environment with borehole imaging and core: a case study from eastern offshore India, International Petroleum Technology Conference, Kuala Lumpur, December

Singha D, Chatterjee R (2017) Rock physics modeling in sand reservoir through well log analysis, Krishna-Godavari basin, India. Geomechanics Eng 13(1):99–117

Weber KJ (1987) Hydrocarbon distribution patterns in Nigerian growth fault structures controlled by structural style and stratigraphy. J Pet Sci Eng 1:91–104